J Neurophysiol 124: 682–690, 2020.
First published July 29, 2020; doi:10.1152/jn.00305.2020.

RESEARCH ARTICLE | *Control of Homeostasis*

Muscle sympathetic single-unit response patterns during progressive muscle metaboreflex activation in young healthy adults

Anthony V. Incognito,[1] Massimo Nardone,[1]* André L. Teixeira,[1]* Jordan B. Lee,[1] Muhammad M. Kathia,[1] and Philip J. Millar[1,2]

[1]*Department of Human Health and Nutritional Sciences, University of Guelph, Guelph, Ontario, Canada; and* [2]*Toronto General Research Institute, Toronto, Ontario, Canada*

Submitted 26 May 2020; accepted in final form 20 July 2020

Incognito AV, Nardone M, Teixeira AL, Lee JB, Kathia MM, Millar PJ. Muscle sympathetic single-unit response patterns during progressive muscle metaboreflex activation in young healthy adults. *J Neurophysiol* 124: 682–690, 2020. First published July 29, 2020; doi:10.1152/jn.00305.2020.—Muscle sympathetic single units can respond differentially to stress, but whether these responses are linked to the degree of sympathoexcitation is unclear. Fifty-three muscle sympathetic single units (microneurography) were recorded in 17 participants (8 women; 24 ± 3 yr). Five 40-s bouts of 10% static handgrip were performed during a 10-min forearm ischemia to progressively increase metabolite accumulation. Each static handgrip was separated by a 75-s ischemic rest [postexercise circulatory occlusion (PECO)] to assess the isolated action of the muscle metaboreflex. During each set of PECO, individual single units were classified as activated, nonresponsive, or inhibited if the spike frequency was above, within, or below the baseline variability, respectively. From *sets 1–5* of PECO, the proportion of single units with activated (34, 45, 68, 87, and 89%), nonresponsive (43, 44, 23, 7, and 9%), or inhibited (23, 11, 9, 6, and 2%) responses changed ($P < 0.001$) as total muscle sympathoexcitation increased. A total of 51/53 (96%) single units were activated in at least one set of PECO, 16 (31%) initially inhibited before activation. This response pattern delayed the activation onset compared with noninhibited units (*set 3 ± 1* vs. *2 ± 1*, $P < 0.001$). Once activated, the spike-frequency rate of rise was similar (8.5 ± 6.5 vs. 7.1 ± 6.0 spikes/min per set, $P = 0.48$). Muscle sympathetic single-unit firing demonstrated differential control during muscle metaboreflex activation. Single units that were initially inhibited during progressive metaboreflex activation were capable of being activated in later sets. These findings reveal that single-unit activity is influenced by convergent neural inputs (i.e., both inhibitory and excitatory), which yield heterogenous single-unit activation thresholds.

NEW & NOTEWORTHY Muscle sympathetic single units respond differentially to sympathoexcitatory stress such that single units can increase firing to contribute to the sympathoexcitatory response or can be nonresponsive or even inhibited. We observed a subgroup of single units that can respond bidirectionally, being first inhibited before activated by progressive increases in forearm muscle metaboreflex activation. These results suggest convergent neural inputs (i.e., inhibitory and excitatory), which yield heterogenous muscle sympathetic single-unit activation thresholds.

microneurography; muscle metaboreflex; sympathetic nervous system

INTRODUCTION

Investigations into the response patterns of muscle sympathetic action potentials underlying integrated multiunit recordings have advanced our understanding of the neural substrates mediating sympathoexcitation during stress. Increases in the total integrated multiunit burst signal [termed total muscle sympathetic nerve activity (MSNA)] during classic experimental stressors (Fagius et al. 1989; Farrell et al. 1991; Hardy et al. 1994; Mark et al. 1985; Sundlöf and Wallin 1978) are now understood to be driven by increases in the number of action potentials occurring across and within cardiac cycles (Macefield and Wallin 2018; Shoemaker 2017). The use of wavelet assessments of muscle sympathetic action potential amplitude clusters (Shoemaker 2017) have demonstrated an important role for ordered, size-dependent recruitment of sympathetic fibers in the control of integrated multiunit burst strength (i.e., burst height and area) at baseline and during sympathoexcitatory stressors (Badrov et al. 2015, 2016; Salmanpour et al. 2011; Steinback et al. 2010). Less understood are the mechanisms underlying muscle sympathetic fiber inhibition and rate coding during sympathoexcitatory stress.

Our group has identified populations of muscle sympathetic fibers (termed single units) that can be inhibited amidst activation of a larger majority of recorded fibers (indicated by increased total MSNA) during lower body negative pressure and rhythmic handgrip exercise (Incognito et al. 2019; Millar et al. 2013, 2015). Similar findings showing patterns of inhibition amidst total MSNA activation have been reported in select action potential amplitude clusters during arterial baroreceptor unloading with lower body negative pressure (Badrov et al. 2015; Salmanpour et al. 2011) and bolus injection of nitroprusside (Limberg et al. 2018). These data have been taken as support for differential control of individual sympathetic fibers directed toward the same target organ (Incognito et al. 2019). Such control is hypothesized to involve an afferent-specific (e.g., cardiovascular afferents) functional arrangement within central autonomic regions supplying sympathetic premotor neurons (Morrison 2001). This hypothesis is informed by animal work that shows rostral ventrolateral medulla (RVLM) subregions to innervate distinct vascular regions throughout the body (Lovick 1987; McAllen and Dampney 1990; Mueller et al. 2011). As well, there exists heterogenous afferent populations with opposing (or differential) discharge

* M. Nardone and A. L. Teixeira contributed equally to this work.
Correspondence: P. J. Millar (pmillar@uoguelph.ca).

patterns (i.e., one subpopulation is inhibited while another subpopulation is activated) in response to single (or homogenous) stimuli (Blair 1986; Folkow 2000; Hainsworth 2014; Oberg and Thorén 1972, 1973; Seagard et al. 1993). Additionally, subpopulations of efferent postganglionic sympathetic nerves can respond selectively (DiBona et al. 1996; DiBona and Sawin 1999; Gregor et al. 1976; Horeyseck et al. 1976) or differentially (Meckler and Weaver 1988; Riedel and Peter 1977; Simon and Riedel 1975) to afferent stimuli.

We observed that inhibition of single units during rhythmic handgrip was almost exclusively present in individuals with small increases in total MSNA during rhythmic handgrip (Incognito et al. 2019). Whether the absence of single-unit inhibition responses in individuals with high levels of sympathoexcitation during exercise is due to unique phenotypic and/or neuroplastic differences within individuals or due to the ability to activate previously inhibited muscle sympathetic fibers during higher levels of stress is unknown. The latter would suggest that both inhibition and activation patterns can be expressed by the same postganglionic fiber in a manner that is threshold dependent.

The present study assessed the influence of progressive muscle metaboreflex activation (potent sympathoexcitatory stimulus) on the response patterns of muscle sympathetic single units. Participants completed a 10-min forearm ischemia, and within the time frame five 40-s bouts of 10% static handgrip were completed, each separated by a 75-s rest [i.e., postexercise circulatory occlusion (PECO)]. The low-intensity static handgrip exercise periods were used to gradually increase the concentration of metabolites trapped within the muscle to elicit a progressive change in muscle metaboreflex activation. We hypothesize that muscle sympathetic fibers can be both inhibited and activated during PECO such that a subgroup of single units will be inhibited during low levels of metaboreflex activation (early sets of the protocol) and will become activated during higher levels of metaboreflex activation (later sets of the protocol). When activated (whether early or late in the protocol), the increase in metaboreflex activation in subsequent sets will drive progressive increases in single-unit spike frequency.

METHODS

Participants. Twenty-four participants volunteered for the study. All participants were young (<40 yr), nonsmoking, unmedicated (not including birth control), in sinus rhythm, and free of known cardiovascular, metabolic, or neuromuscular diseases. Women were tested during the early follicular phase (*day 0–5*) or placebo week of their natural or controlled menstrual cycle, respectively. Due to scheduling difficulties, one woman was tested on *day 6* of her natural menstrual cycle. All participants were familiarized to the ischemic handgrip exercise protocol 24 h or longer before the testing visit. The University of Guelph Research Ethics Board approved all study procedures, and all participants provided informed written consent before familiarization and testing visits.

Measurements. Discrete minute-to-minute blood pressure was measured using an automated oscillometric blood pressure cuff over the right upper arm (BPTru Medical Devices, Coquitlam, Canada). Continuous measures of heart rate (lead II electrocardiography; ADInstruments Inc, Colorado Springs, CO), blood pressure (photoplethysmography cuff on the left third digit; Finometer MIDI, Finapres Inc, The Netherlands), respiratory excursions (piezoelectric transducer belt placed around the thorax; Pneumotrace II, UFA, Morro Bay, CA), forearm oxygenated and deoxygenated hemoglobin [near-infrared spectroscopy (NIRS) optode (Artinis Medical Systems) placed and secured on the medial aspect of the supinated forearm ~3–4 cm distal to the medial epicondyle and covered with an opaque cloth], and MSNA (microneurography) were monitored throughout the experiment. A handgrip dynamometer (MLT004/ ST; ADInstruments, Sydney, NSW, Australia) was used to measure handgrip force output and to provide real-time digital feedback to ensure appropriate exercise intensities were achieved during testing. All continuous data (except NIRS data) were digitized and stored (ADInstruments Inc, Colorado Springs, CO) at a sampling frequency of 1 kHz, except for the raw MSNA signal, which was sampled at 20 kHz. NIRS data were sampled at 10 Hz (downsampled to 1 Hz for analysis). Total hemoglobin was calculated as the absolute sum of oxygenated and deoxygenated hemoglobin. Oxygenated and deoxygenated hemoglobin were analyzed separately and normalized to the individual range of each variable, calculated as the minimum and maximum values recorded from 30-s epochs throughout the entire protocol (from the 6-min baseline to the 3-min recovery). A 10-min occlusion with concurrent ischemic exercise followed by a 3-min reperfusion period is likely to produce maximal (or near maximal) ranges of hemoglobin oxygenation and deoxygenation values (Inglis et al. 2017).

Multiunit and single-unit muscle sympathetic nerve activity (MSNA) was recorded from the fibular nerve, as previously described (Millar et al. 2013; Notay et al. 2016). A high-impedance tungsten microelectrode (FHC, Bowdoin, ME) was inserted posterior and slightly distal to the fibular head with the knee flexed ~30° and adjacent to a low-impedance reference electrode inserted beneath the skin surface. The raw MSNA neurogram was amplified (75,000 times) and bandpass filtered (0.7– 2.0 kHz), and the multiunit MSNA neurogram was rectified and integrated using a 0.1-s time constant (Nerve Traffic Analyzer, model 662C-4; Absolute Designs, Iowa City, IA). Muscle sympathetic nerve traffic was identifiable by pulse-synchronous burst patterns and amplified by voluntary apnea. Absence of skin sympathetic nerve traffic was confirmed by lack of responsiveness to unexpected clapping. To ensure stability of the nerve recording, 7–10 min were given to monitor the neurogram without microelectrode manipulation. Once a high-quality nerve recording was confirmed (signal-to-noise ratio $\geq$ 3:1 with no baseline noise drift), the experimental protocol commenced. During the study protocol, if there was a potential change in the site recording, the protocol was stopped and restarted after 15–20 min of rest. The study was terminated if the nerve recording could not be found or was repeatedly compromised during the protocol.

Multiunit MSNA was analyzed using a custom semiautomated LabView software program (National Instruments, Austin, TX), as described previously (Millar et al. 2013; Notay et al. 2016). Multiunit MSNA was quantified with the following variables: burst frequency (bursts/min), burst incidence (bursts/100 heartbeats), normalized burst height (relative to peak baseline height), total MSNA (normalized mean burst area $\times$ burst frequency), and burst latency (ECG R spike to burst peak). Single-unit MSNA was analyzed using Spike2 (v7; Cambridge Electronics Design Ltd, Cambridge, UK), as described previously (Incognito et al. 2019; Millar et al. 2013). Spikes displaying a triphasic morphology with a negative amplitude deflection visually inspected to be larger than the noise width and active during the resting baseline were subject to single-unit classification. With the use of previously published criteria (Macefield et al. 2002; Murai et al. 2006, 2009), candidate single units were matched by amplitude of the negative deflection and waveform shape to yield minimal variation in waveform overlays. Single-unit MSNA was quantified with the following variables: spike frequency (spikes/min), spike incidence (spikes/100 heartbeats), probability of spike firing one or more times per cardiac cycle (%), probability of multiple spike firing within a cardiac cycle (%), and spike onset latency (ECG R spike to first spike; ms) (Macefield et al. 2002; Murai et al. 2006, 2009). Baseline spike frequency was used as an inverse index of postganglionic fiber size

(Incognito et al. 2019; Salmanpour et al. 2011). All MSNA analyses were completed by a single investigator (A.V.I.).

Experimental protocol. Participants arrived at the laboratory after voiding and abstaining from caffeine, alcohol, recreational drugs, and strenuous exercise for 20–24 h. All testing was performed in a supine position with the upper body elevated slightly (~10–20°) to permit view of handgrip force output on a computer screen. Prior to instrumentation, participants performed two maximal volitional handgrip contractions (MVC) in the right hand separated by 60 s of rest. The effort yielding the highest force output was used as the MVC. Following instrumentation, participants rested for 10 min before undergoing a 6-min baseline period. The oscillometric blood pressure cuff on the right upper arm was then replaced with a manual sphygmomanometer and inflated to suprasystolic pressure (240 mmHg) for 10 min. During the 10-min period of blood flow occlusion, participants performed five sets of 40-s static handgrip at 10% MVC. After each bout, 75 s of ischemic rest were completed and labeled as postexercise circulatory occlusion (PECO). The low-intensity static handgrip exercise periods were used to increase the concentration of metabolites trapped within the muscle to elicit a progressive change in muscle metaboreflex activation. NIRS measures of total hemoglobin (oxygenated + deoxygenated hemoglobin) were used to assess whether additional blood entered the forearm during the occlusion. NIRS measures of oxygenated and deoxygenated hemoglobin were obtained to confirm that oxidative metabolism was continuous throughout the protocol. The first handgrip set began 25 s after the inflation of the cuff. Prior to each handgrip set, participants were given a 5-s countdown. Following deflation of the manual sphygmomanometer cuff, participants were given 3–4 min of rest before completing a maximal end-expiratory voluntary apnea.

Data and statistical analysis. Mean values of all NIRS, hemodynamic, and MSNA variables were calculated for the baseline period and during PECO (10–70 s of each 75-s occlusion set). Mean values of all hemodynamic and MSNA variables were also calculated for the last 20% of maximal end-expiratory apnea time. We classified single-unit responses for each set of PECO as either activated, nonresponsive, or inhibited based on whether the spike frequency during each set was above, within, or below the range of 1-min absolute values observed in the baseline period, respectively. We selected 3 min of baseline measures (three 1-min time points) to quantify these response thresholds to align with prior work (Incognito et al. 2019). Using this method, we quantified the activation threshold of each single unit, defined as the first set that elicited an increase in spike frequency above the highest active minute recorded in the baseline. Furthermore, we also quantified the responsiveness to muscle metaboreflex-mediated activation in each single unit as the rate of rise in spike frequency once activated. This variable was quantified as the linear regression slope between spike frequency and set number (termed the activation slope). The sets used for the regression analysis were the set immediately preceding the first set of activation (activation threshold) and *set 5*. Given the variability in the activation threshold, this yielded variability in the number of points used for each regression. To allow for assessments of single units that were activated in *set 5* ($n = 3$), only two points were used (*set 4* and *set 5*). All other slopes had a minimum of three points, and only single units with strong ($r \geq 0.60$) linear regressions were used. We also assessed whether common response patterns over time were apparent in each set of PECO. We defined two general response patterns and grouped single units into those that were inhibited in early sets of the protocol before becoming activated in later sets (termed initially inhibited single units) or those that were not inhibited in any set of PECO (only nonresponsive or activated; termed noninhibited single units).

One-way ANOVAs with repeated measures were used to quantify responses of all NIRS, hemodynamic, and multi- and single-unit MSNA variables during the experimental protocol. A Fisher's exact probability test was used to compare proportional differences in activated, nonresponsive, and inhibited single-unit responses across all five sets of PECO. Unpaired Student's *t* tests were used to compare the baseline spike frequency, spike-frequency response to maximal end-expiratory apnea, activation threshold, and the activation slope between the initially inhibited and noninhibited single units, as well as the baseline characteristics between individuals with and without initially inhibited single units. Two-way ANOVAs with repeated measures were used to quantify the spike-frequency difference between the two single-unit subgroups throughout the five sets of PECO [group (initially inhibited vs. noninhibited single units) × time (set number)], as well as the NIRS (data expressed as change from baseline), hemodynamic, and multiunit MSNA responses in the individuals that possessed and did not possess initially inhibited single units. Pearson correlational analyses assessed the relationship between variables of interest. Bonferroni post hoc procedures were performed on all ANOVA analyses with significant interaction effects. All analyses were performed using IBM SPSS Statistics 23 (Armonk, NY). Significance level was set at $P < 0.05$, and all data are presented as means ± SD, unless otherwise stated.

RESULTS

Complete data were obtained in 17 (8 women) participants [age: 24 ± 3 yr; height: 170 ± 10 cm; weight: 72 ± 15 kg; body mass index (BMI): 25 ± 3 kg/m^2]. The remaining seven were excluded due to an inability to find an MSNA site or hold a stable site during the protocol. Representative data across the entire study protocol from one participant are shown in Fig. 1.

NIRS, hemodynamic, and multiunit MSNA responses. Total hemoglobin, oxygenated and deoxygenated hemoglobin, heart rate, blood pressure, and multiunit MSNA responses are summarized in Table 1. Total hemoglobin was maintained at levels similar to baseline throughout the protocol (all $P > 0.99$). Muscle oxygenation and deoxygenation reached a maximal decrease ($\Delta -70 \pm 20\%$, $P < 0.001$) and increase ($\Delta 81 \pm 9\%$, $P < 0.001$) from baseline in *sets 4* and *5* of PECO, respectively. Heart rate ($\Delta 4 \pm 4$ beats/min, $P = 0.01$) and blood pressure (systolic and diastolic: $\Delta 6 \pm 4$ and $\Delta 4 \pm 3$ mmHg, both $P \leq 0.008$) were increased above baseline by *set 1* of PECO. Multiunit MSNA burst frequency (*set 2*: $\Delta 5 \pm 6$ bursts/min, $P = 0.06$), burst incidence (*set 3*: $\Delta 11 \pm 8$ bursts/100 heartbeats, $P = 0.001$), burst height (*set 3*: $\Delta 5 \pm 4\%$ of baseline peak, $P = 0.002$), and total MSNA (*set 2*: $\Delta 164 \pm 205$ arbitrary units/min, $P = 0.07$) were increased from baseline by *sets 2–3* of PECO (Table 1).

Muscle sympathetic single-unit responses. A total of 53 single units were identified [number of single units per participant: one ($n = 2$); two ($n = 4$); three ($n = 4$); four ($n = 4$); five ($n = 3$)]. Figure 2 demonstrates the proportion of single units during *sets 1* to *5* that were activated (34, 45, 68, 87, and 89%), nonresponsive (43, 44, 23, 7, and 9%), or inhibited (23, 11, 9, 6, and 2%) throughout the protocol. The proportion of activated ($r = 0.95$, $P = 0.02$), nonresponsive ($r = -0.93$, $P = 0.02$), and inhibited ($r = -0.86$, $P = 0.06$) single units were linearly related to the percent change in multiunit total MSNA in each set. For comparison, the last 20% of the maximal end-expiratory apnea yielded higher total MSNA than *set 5* of PECO ($\Delta 1{,}505 \pm 1{,}447$ vs. $\Delta 161 \pm 79$ arbitrary units/min, $P < 0.001$) and 100% of single units were activated. The remaining analyses were based on the 51 (96%) single units that were activated in at least one set of PECO. Mean single-unit MSNA response data are summarized in Table 1. Spike frequency (*set 2*: $\Delta 3 \pm 6$ spikes/min, $P = 0.05$), spike incidence (*set 3*: $\Delta 14 \pm 22$ spikes/100 heartbeats, $P < 0.001$),

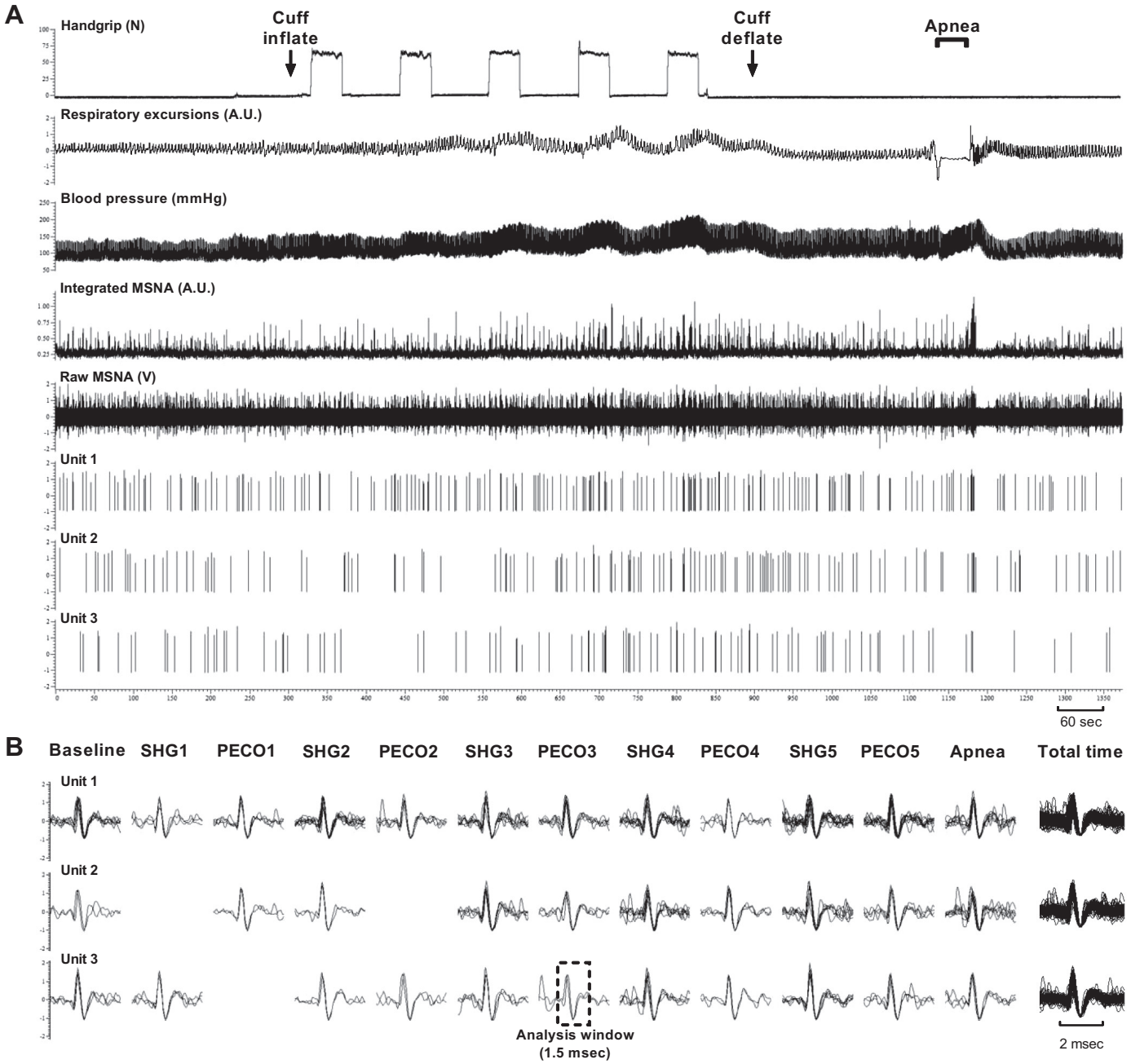

Fig. 1. *A*: representative recording of handgrip force, arterial pressure, and multi- and single-unit muscle sympathetic nerve activity (MSNA) during baseline, the ischemic handgrip protocol, and a maximal end-expiratory voluntary apnea. *B*: overlaid spike waveforms for each single unit across 30-s epochs in each phase of the experimental protocol [i.e., baseline, static handgrip (SHG), postexercise circulatory occlusion (PECO), apnea] and across the whole experimental protocol [i.e., total time (23 min)] to show the typical variability within each waveform template. Spike waveform parameters that were matched over time fell within a 1.5-ms time window. Absent waveforms for *unit 2* during *set 1* of SHG and *set 2* of PECO and for *unit 3* during *set 1* of PECO are the result of a lack of firing of each respective single unit during the protocol phases. A.U., arbitrary units; N, newtons; V, volts.

spike probability (set 3: $\Delta 6 \pm 8\%$/cardiac cycle, $P < 0.001$), and probability of multiple spike firing (*set 4*: $\Delta 8 \pm 15\%$, $P = 0.01$) were increased from baseline by *sets 2–4* of PECO.

Muscle sympathetic single-unit response pattern subgroups. We identified 16 (31%) single units that were initially inhibited before activation (Fig. 3, open circles for examples). Baseline spike frequency was not different between the initially inhibited vs. noninhibited single units (15 ± 13 vs. 19 ± 17 spikes/min, $P = 0.42$), nor was the spike frequency during maximal end-expiratory apnea (176 ± 175 vs. 253 ± 197, $P = 0.19$). When assessing the activation threshold of each single unit (the set number when the spike frequency was first greater than the highest active minute recorded in the baseline), we observed the initially inhibited single units to have a delayed onset of activation or a higher activation threshold (*set 3* $\pm$ *1* vs. *2* $\pm$ *1*, $P < 0.001$; Fig. 4*A*). This observation was also apparent when the mean responses of the single-unit subgroups were compared, which showed the spike frequency of the initially inhibited single units to be increased above baseline in *set 5* ($\Delta 14 \pm 12$ spikes/min, $P = 0.001$) compared with *set 3*

Table 1. *NIRS, hemodynamic, and MSNA responses to progressive isolated muscle metaboreflex activation*

	Baseline	*Set 1*	*Set 2*	*Set 3*	*Set 4*	*Set 5*
NIRS						
Total hemoglobin, A.U.	43 ± 9	44 ± 10	44 ± 10	42 ± 9	41 ± 8	41 ± 8
Oxy. hemoglobin, %max range	66 ± 16	42 ± 16*	21 ± 10*†	11 ± 7*†	6 ± 5*†	7 ± 9*
Deoxy. hemoglobin, %max range	13 ± 6	58 ± 9*	86 ± 7*†	93 ± 5*†	93 ± 6*	94 ± 6*
Hemodynamics						
Heart rate, beats/min	64 ± 11	68 ± 12*	69 ± 12*	69 ± 12*	69 ± 12*	68 ± 12§
SBP, mmHg	106 ± 9	113 ± 11*	117 ± 12*†	120 ± 16*	125 ± 14*†	130 ± 16*†
DBP, mmHg	67 ± 7	71 ± 8*	74 ± 7*†	76 ± 8*†	79 ± 8*†	83 ± 8*†
Multiunit MSNA						
Burst frequency, bursts/min	18 ± 7	18 ± 8	22 ± 10§	26 ± 8*	30 ± 8*	34 ± 9*†
Burst incidence, bursts/100 heartbeats	28 ± 12	28 ± 13	33 ± 15	39 ± 14*	43 ± 12*	50 ± 14*†
Burst height, %baseline peak	47 ± 11	51 ± 16	48 ± 12	52 ± 12*	57 ± 14*†	62 ± 18*
Total MSNA, A.U.	684 ± 280	762 ± 340	849 ± 355§	1,079 ± 355*†	1,313 ± 311*†	1,639 ± 398*†
Burst latency, ms	1,300 ± 91	1,302 ± 92	1,308 ± 93	1,311 ± 85	1,305 ± 96	1,296 ± 104
Single-unit MSNA						
Spike frequency, spikes/min	18 ± 16	20 ± 19	21 ± 19*	28 ± 24*†	35 ± 30*†	41 ± 34*†
Spike incidence, spikes/100 heartbeats	30 ± 30	33 ± 33	32 ± 31	44 ± 40*†	54 ± 50*†	66 ± 58*†
Spike probability, %/cardiac cycle	17 ± 12	18 ± 13	18 ± 12	24 ± 15*†	27 ± 15*†	31 ± 17*†
Prob. multiple spike firing, %	28 ± 19	31 ± 25	26 ± 24	31 ± 24	35 ± 24*	39 ± 24*
Spike onset latency, ms	1,202 ± 107	1,197 ± 115	1,201 ± 125	1,200 ± 129	1,199 ± 122	1,175 ± 136*†

Values are means ± SD. Heart rate, blood pressure, and multi- and single-unit muscle sympathetic nerve activity (MSNA) responses to the experimental protocol were analyzed using one-way ANOVAs with repeated measures in 17 participants and 51 single units. No bursts or spikes were recorded during at least one time period in 1 participant and 2 single units, thus the burst height and latency analysis had 16 participants and spike onset latency analyses were performed on 49 single units. A.U., arbitrary units; DBP and SBP, diastolic and systolic blood pressure; NIRS, near-infrared spectroscopy; Oxy. and Deoxy., oxygenated and deoxygenated; Prob., probability. *$P < 0.05$, §$P \leq 0.07$ vs. baseline; †$P \leq 0.05$ vs. previous set.

($\Delta 15 \pm 13$ spikes/min, $P < 0.001$) in the noninhibited single units (Fig. 4*B*).

The proportion of single units with strong linear regression slopes ($r \geq 0.60$) when the rate of rise in spike frequency was evaluated did not differ between initially inhibited vs. noninhibited single-unit subgroups [13/16 (81%) vs. 31/35 (89%), $P = 0.66$], nor did the slopes (8.5 ± 6.5 vs. 7.1 ± 6.0 spikes/min/set, $P = 0.48$; Fig. 4*C*). The magnitude of maximal activation (greatest Δ from baseline in spike frequency achieved during the protocol) was significantly lower in the initially inhibited vs. noninhibited single units ($\Delta 16 \pm 11$ vs. 30 ± 24 spikes/min, $P = 0.03$), which was expected given the higher activation threshold and similar rate of rise in spike frequency. Noteworthy, the magnitude of activation at the activation threshold was not different between single-unit subgroups ($\Delta 7 \pm 7$ vs. 11 ± 9 spikes/min, $P = 0.18$). Lastly, in the initially inhibited single units, baseline spike frequency was correlated to the magnitude of inhibition ($r = -0.76$, $P < 0.001$), the magnitude of activation at the activation threshold ($r = 0.58$, $P = 0.02$), and the magnitude of maximal activation ($r = 0.58$, $P = 0.02$). Similarly, in the noninhibited single units, baseline spike frequency was related to the magnitude of activation at the activation threshold ($r = 0.41$, $P = 0.02$) and the magnitude of maximal activation ($r = 0.66$, $P < 0.001$).

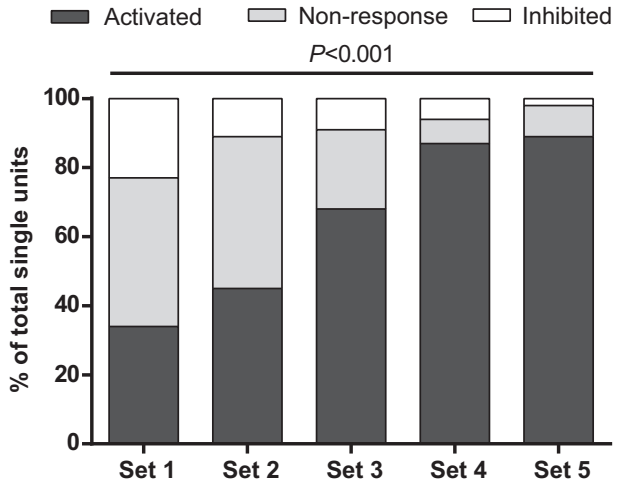

Fig. 2. Contingency table showing the proportion of single units identified to be activated, nonresponsive, or inhibited during 5 sets of muscle metaboreflex activation using postexercise circulatory occlusion. Fisher's exact probability test was used to assess proportional changes.

At least one initially inhibited single unit was observed in seven participants (3 women). Individuals with initially inhibited single units compared with individuals with only noninhibited single units had an attenuated rise in deoxygenated hemoglobin in *sets 1*, *2*, and *3* of PECO (*set 1*: $\Delta 38 \pm 10$ vs. $\Delta 50 \pm 14$, $P = 0.02$; *set 2*: $\Delta 67 \pm 10$ vs. $\Delta 78 \pm 7$, $P = 0.02$; *set 3*: $\Delta 75 \pm 7$ vs. $\Delta 85 \pm 6$% of maximal range, $P = 0.07$), corresponding to a delayed increase from baseline in MSNA burst frequency [*set 4*: $\Delta 8 \pm 5$ ($P < 0.001$) vs. *set 2*: $\Delta 6 \pm 5$ bursts/min ($P = 0.002$)], burst incidence [*set 4*: $\Delta 10 \pm 7$ ($P = 0.01$) vs. *set 2*: $\Delta 8 \pm 7$ bursts/100 heartbeats ($P = 0.03$)], and total MSNA [*set 3*: $\Delta 243 \pm 174$ ($P = 0.08$) vs. *set 1*: $\Delta 232 \pm 197$ arbitrary units/min ($P = 0.02$)].

DISCUSSION

This study sought to investigate response patterns of muscle sympathetic single units during progressive muscle metaboreflex activation, evoked with intermittent periods of ischemic static handgrip. Nearly all single units [51/53 (96%)] were activated by the muscle metaboreflex, albeit at varying sets of PECO. The fourth and fifth sets of PECO yielded the greatest proportion of single units that were activated (i.e., with activity levels above baseline variability; 87 and 89% of single units, respectively), which coincided with the greatest reductions and elevations in oxygenated and deoxygenated hemoglobin, re-

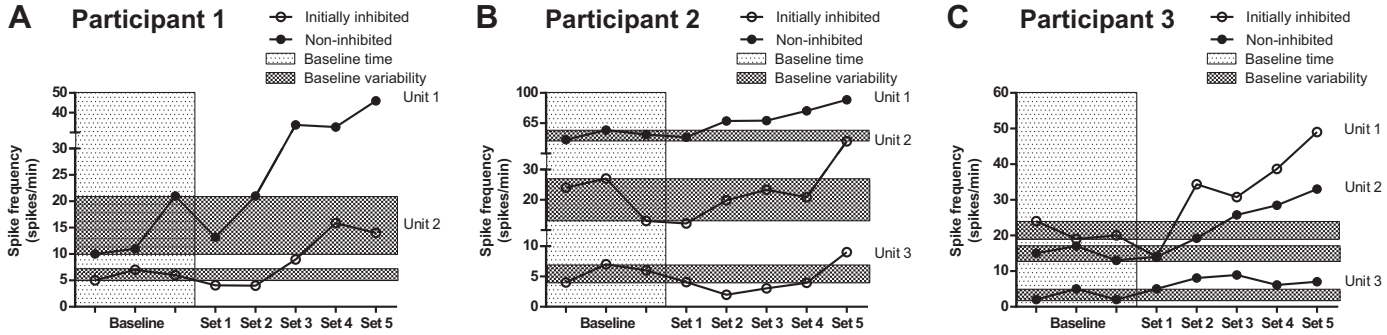

Fig. 3. Identifying response patterns during progressive muscle metaboreflex activation. *A–C*: single-unit response patterns from 3 participants. Light shaded area indicates the baseline epoch. Dark shaded area indicates the minute-to-minute baseline variability used to identify activation, nonresponse, and inhibition in *sets 1–5*. Responses were classified as activated, nonresponsive, or inhibited for each set if activity was above, within, or below the baseline variability band, respectively. We identified 2 general response patterns: initially inhibited (open circles) and noninhibited (filled circles) single units.

spectively. A minority of single units [16/51 (31%)] underwent inhibition before being activated. This single-unit subgroup had higher metaboreflex activation thresholds, evident by their delayed onset of activation during the protocol, yet a similar rate of rise in spike frequency to noninhibited single units once activated. Our findings reveal a subgroup of single units with bidirectional response patterns, which suggests that both inhibitory and excitatory neural inputs can simultaneously influence sympathetic single unit activity.

In our prior work, we identified single units with heterogenous response patterns to rhythmic handgrip exercise. Interestingly, single units undergoing inhibition during rhythmic handgrip were nearly absent in individuals with the largest integrated MSNA response (Incognito et al. 2019). As we did not assess whether single-unit activity could change response directionality over time, it was unclear as to whether these observations were due to interindividual differences in single-unit phenotypes or due to differential response thresholds of each single unit. The present study demonstrates clearly that all single units can be activated given a threshold level of sympathoexcitation. Under low levels of sympathoexcitation (quantified by the integrated total MSNA response), there is a proportion of single units with inhibitory response patterns. As sympathoexcitation increases, we see a progressive shift toward an activation response (increase in spike frequency) of nearly all single units, with a subpopulation of single units shifting from being inhibited to activated. Moreover, all single units were activated during maximal end-expiratory apnea, which elicited a more potent sympathoexcitatory response compared with the progressive muscle metaboreflex protocol.

Currently, differential control has been postulated to be governed by distinct neural pathways (Morrison 2001). This model was recently portrayed as an axonal ribbon cable, whereby a single neural afferent pathway [arising from a specific cardiovascular receptor (i.e., baroreceptor, chemoreceptor)] synapses in the brain stem on a neuron(s) that directly influences a single sympathetic efferent pathway (Zera et al. 2019). The organizational framework of this model arises from evidence of RVLM neurons (as well as others) with dedicated innervations to regionally (Lovick 1987), viscerally (McAllen et al. 1995; McAllen and Dampney 1990; Mueller et al. 2011), and functionally (Farmer et al. 2019) distinct end-target organs, alongside evidence of heterogenous afferent responsiveness to single stimuli (Blair 1986; Folkow 2000; Seagard et al. 1993). Though potentially relevant in the context of inter-organ differential control, the relevance of this mode of control of postganglionic fibers directed toward a functionally similar single target organ is unlikely. Our observation of a subpopulation of muscle sympathetic single units that underwent inhibition before being activated by progressive muscle metaboreflex stress argues against a model where distinct supraspinal neural pathways are solely responsible for differential control of postganglionic muscle sympathetic fibers (i.e., the capacity for only inhibited or activated single-unit response patterns throughout the protocol). Instead, it suggests that this level of differential control is regulated by supraspinal convergence and weighting of multiple inhibitory and excitatory neural inputs to produce differential inhibition and activation response thresholds. We hypothesize that single-unit inhibition before activation is due to inhibitory baroreceptor inputs that compete

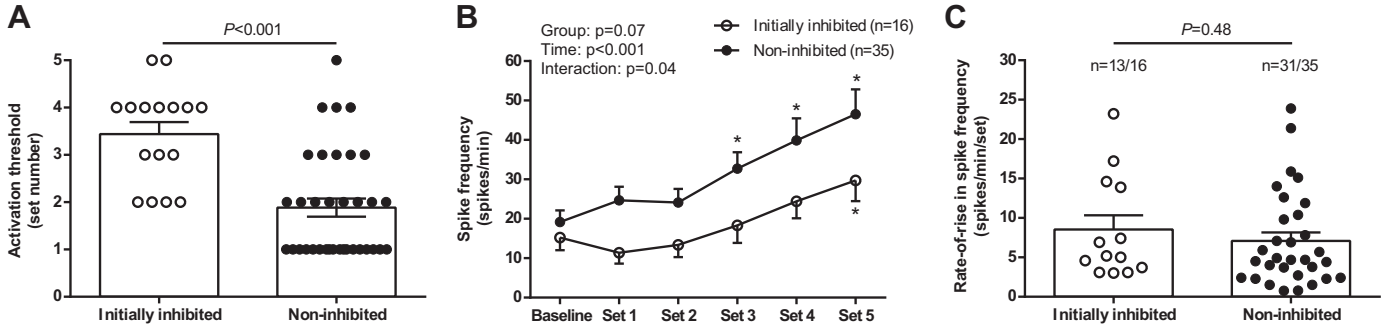

Fig. 4. Characteristics of activation in 2 single-unit response pattern subgroups. *A*: mean differences in the activation threshold compared using an unpaired Student's *t* test. *B*: mean spike frequency compared using a 2-way ANOVA with repeated measures. *C*: the activation slope, which is the linear regression slope of spike frequency and set number, compared using an unpaired Student's *t* test. Data are means ± SE. $^*P < 0.05$ vs. baseline.

with excitatory muscle metaboreceptor inputs. The point of convergence (or competition) has been postulated to be within the nucleus tractus solitarii (NTS), whereby muscle metaboreflex afferents inhibit arterial baroreflex inhibition of sympathetic outflow through GABAergic transmission (Teixeira et al. 2020).

There is a high degree of neural input convergence within the NTS (Andresen and Kunze 1994; Andresen and Peters 2008; Boscan et al. 2002; McDougall et al. 2009; McDougall and Andresen 2013; Paton 1999) and a strong influence of NTS neurons on sympathetic premotor neurons (Aicher et al. 1995; Boscan et al. 2002; Ross et al. 1985). There is also evidence of neural afferent input summation that showcases the functional implications of input convergence in supraspinal regions. Sympathetic responses have been shown to be augmented during the application of multiple sympathoexcitatory stimuli (Cui et al. 2001, 2002; Farrell et al. 1991; Seals et al. 1991), as well as attenuated during the simultaneous application of sympathoinhibitory and sympathoexcitatory stimuli (Chruścielewski et al. 1981; Katayama et al. 2016, 2018; Somers et al. 1991). Furthermore, case reports have shown a paradoxical withdrawal of multiunit MSNA during severe hypotensive stressors (Converse et al. 1992; Scherrer et al. 1990; Wallin and Eckberg 1982), which suggests that all muscle sympathetic single units can lose their negative feedback relationship with arterial blood pressure and the arterial baroreflex. In support, we observed a small number of muscle sympathetic single units to have positive relationships with diastolic blood pressure when pharmacologically driven outside of normal resting arterial baroreflex operating ranges (Incognito et al. 2020). These observations may be mediated by a shift in dominant negative feedback control from arterial baroreceptors to positive feedback control by cardiopulmonary baroreceptors (Dorward et al. 1985; Folkow 2000; Oberg and Thorén 1972, 1973; Simpson et al. 2020), made possible through simultaneous influence of multiple convergent neural inputs.

The magnitude of responses, whether inhibited or activated, were related to the baseline spike frequency, a proxy of postganglionic fiber size (Incognito et al. 2019; Salmanpour et al. 2011), whereby the largest responses occurred in the smallest single units (highest baseline activity). These observations suggest a size-dependent order of rate coding, which complements previous work of a size-dependent order of recruitment (Shoemaker 2017; Steinback et al. 2010). Interestingly, single units that underwent inhibition before activation were of similar fiber size to single units that were only activated. This suggests that size-dependent, ordered response magnitudes are dictated at the level of the paravertebral ganglia, as previously shown (Klassen et al. 2018), whereas response directionality is dictated upstream and within the central circuitry (supraspinal regulatory regions). We also observed that once single units were activated, the rate of rise in spike frequency was similar between initially inhibited and noninhibited single units. This indicates that the inhibitory influences on progressive muscle metaboreflex activation maintained a consistent influence over single-unit activity in each response pattern subgroup. We speculate that single units with initial inhibition patterns are governed by baroreflex neurons with high-threshold metaboreceptor inputs, given the known synaptic influence of metaboreceptor afferents on baroreceptor neurons in the NTS (Teixeira et al. 2020). Once the high-threshold metaboreceptors are activated, a progressive ordered inhibition of inhibitory baroreflex neurons then commences. Further work is warranted to understand the integration of metaboreceptor and baroreceptor neural inputs.

There are several limitations in the present study to consider. First, our ability to classify and match single-unit waveforms requires large-amplitude deflection from the baseline noise width. It is unknown as to whether these responses are representative of the entire postganglionic sympathetic fiber pool. However, our recent work has shown that a large majority of single units are under strong arterial baroreflex control (Incognito et al. 2020), which parallels findings using action potential denoising methods, which are capable of identifying a larger number of waveform amplitude clusters (Klassen et al. 2020; Salmanpour and Shoemaker 2012). Second, we confirmed in this study that the level of sympathoexcitation dictates response directionality of MSNA single units. There exists a large heterogeneity in the sympathoexcitatory level achieved between individuals, and therefore, each single unit recorded was influenced by the overall metaboreflex response in each individual. Indeed, individuals with initially inhibited single units ($n = 7$) had a delay (*set 1* vs. *set 3*) in the increase in the total integrated MSNA above baseline compared with individuals without initially inhibited single units. Though this provides further support of our individual single-unit responses being representative of the function of a larger neuronal pool, it reveals that comparisons of single-unit response patterns between groups must be cautioned in future works if sympathoexcitation level is unmatched. Finally, despite strong support from our previous studies, the mechanistic explanations of our observations remain speculative as they have not been tested directly. Future investigations should aim to prove the validity of these mechanistic hypotheses underlying differential control of sympathetic outflow.

In conclusion, we demonstrate that individual muscle sympathetic single units can be both inhibited and activated in response to progressive muscle metaboreflex stress, which suggests that both inhibitory and excitatory neural inputs can simultaneously influence muscle sympathetic single-unit activity. Once top-down inhibition or activation is initiated, the magnitude of the response is then dependent on the size of the postganglionic fiber, with smaller fibers possessing greater response magnitudes. The degree of sympathoexcitation required to activate an individual postganglionic fiber may be influenced by the strength of convergent inhibitory neural inputs, whereby a high level of excitatory neural input is needed to override strong inhibitory neural inputs governing subgroups of sympathetic efferents. The findings open new hypotheses on the mechanistic underpinnings of differential sympathetic control. Inhibition or activation of a specific sympathetic efferent may be dependent on heterogenous supraspinal activation thresholds, influenced by the unique summative milieu of multiple convergent neural inputs.

GRANTS

A.V.I. was supported by a Natural Science and Engineering Research Council (NSERC) of Canada graduate scholarship. M.N. was supported by an Ontario graduate scholarship. J.B.L. was supported by an NSERC of Canada graduate scholarship. P.J.M. was supported by NSERC Discovery Grant 06019, Canada Foundation for Innovation Grant 34379, Ontario Ministry of

Research, Innovation, and Science Grant 34379, and Ontario Early Researcher Award 18-14-288.

DISCLOSURES

No conflicts of interest, financial or otherwise, are declared by the authors.

AUTHOR CONTRIBUTIONS

A.V.I. and P.J.M. conceived and designed research; A.V.I., M.N., A.L.T., J.B.L., M.M.K., and P.J.M. performed experiments; A.V.I. and J.B.L. analyzed data; A.V.I., and P.J.M. interpreted results of experiments; A.V.I. prepared figures; A.V.I. and P.J.M. drafted manuscript; A.V.I., M.N., A.L.T., and P.J.M. edited and revised manuscript; A.V.I., M.N., A.L.T., J.B.L., M.M.K., and P.J.M. approved final version of manuscript.

REFERENCES

Aicher SA, Kurucz OS, Reis DJ, Milner TA. Nucleus tractus solitarius efferent terminals synapse on neurons in the caudal ventrolateral medulla that project to the rostral ventrolateral medulla. *Brain Res* 693: 51–63, 1995. doi:10.1016/0006-8993(95)00660-I.

Andresen MC, Kunze DL. Nucleus tractus solitarius—gateway to neural circulatory control. *Annu Rev Physiol* 56: 93–116, 1994. doi:10.1146/annurev.ph.56.030194.000521.

Andresen MC, Peters JH. Comparison of baroreceptive to other afferent synaptic transmission to the medial solitary tract nucleus. *Am J Physiol Heart Circ Physiol* 295: H2032–H2042, 2008. doi:10.1152/ajpheart.00568.2008.

Badrov MB, Olver TD, Shoemaker JK. Central vs. peripheral determinants of sympathetic neural recruitment: insights from static handgrip exercise and postexercise circulatory occlusion. *Am J Physiol Regul Integr Comp Physiol* 311: R1013–R1021, 2016. doi:10.1152/ajpregu.00360.2016.

Badrov MB, Usselman CW, Shoemaker JK. Sympathetic neural recruitment strategies: responses to severe chemoreflex and baroreflex stress. *Am J Physiol Regul Integr Comp Physiol* 309: R160–R168, 2015. doi:10.1152/ajpregu.00077.2015.

Blair RW. Cardiac input to medullary reticular formation: neuronal responses to mechanical stimuli. *Am J Physiol Regul Integr Comp Physiol* 251: R680–R689, 1986. doi:10.1152/ajpregu.1986.251.4.R680.

Boscan P, Pickering AE, Paton JF. The nucleus of the solitary tract: an integrating station for nociceptive and cardiorespiratory afferents. *Exp Physiol* 87: 259–266, 2002. doi:10.1113/eph8702353.

Chruścielewski L, Majcherczyk S, Trzebski A. The effect of activation of carotid body chemoreceptors on baroreceptor inhibition of sympathetic activity. *Acta Neurobiol Exp (Wars)* 41: 175–187, 1981.

Converse RL Jr, Jacobsen TN, Jost CM, Toto RD, Grayburn PA, Obregon TM, Fouad-Tarazi F, Victor RG. Paradoxical withdrawal of reflex vasoconstriction as a cause of hemodialysis-induced hypotension. *J Clin Invest* 90: 1657–1665, 1992. doi:10.1172/JCI116037.

Cui J, Wilson TE, Crandall CG. Baroreflex modulation of muscle sympathetic nerve activity during cold pressor test in humans. *Am J Physiol Heart Circ Physiol* 282: H1717–H1723, 2002. doi:10.1152/ajpheart.00899.2001.

Cui J, Wilson TE, Shibasaki M, Hodges NA, Crandall CG. Baroreflex modulation of muscle sympathetic nerve activity during posthandgrip muscle ischemia in humans. *J Appl Physiol (1985)* 91: 1679–1686, 2001. doi:10.1152/jappl.2001.91.4.1679.

DiBona GF, Sawin LL. Renal hemodynamic effects of activation of specific renal sympathetic nerve fiber groups. *Am J Physiol Regul Integr Comp Physiol* 276: R539–R549, 1999. doi:10.1152/ajpregu.1999.276.2.R539.

DiBona GF, Sawin LL, Jones SY. Differentiated sympathetic neural control of the kidney. *Am J Physiol* 271: R84–R90, 1996. doi:10.1152/ajpregu.1996.271.1.R84.

Dorward PK, Riedel W, Burke SL, Gipps J, Korner PI. The renal sympathetic baroreflex in the rabbit. Arterial and cardiac baroreceptor influences, resetting, and effect of anesthesia. *Circ Res* 57: 618–633, 1985. doi:10.1161/01.RES.57.4.618.

Fagius J, Karhuvaara S, Sundlöf G. The cold pressor test: effects on sympathetic nerve activity in human muscle and skin nerve fascicles. *Acta Physiol Scand* 137: 325–334, 1989. doi:10.1111/j.1748-1716.1989.tb08760.x.

Farmer DG, Pracejus N, Dempsey B, Turner A, Bokiniec P, Paton JF, Pickering AE, Burguet J, Andrey P, Goodchild AK, McAllen RM, McMullan S. On the presence and functional significance of sympathetic premotor neurons with collateralized spinal axons in the rat. *J Physiol* 597: 3407–3423, 2019. doi:10.1113/JP277661.

Farrell PA, Ebert TJ, Kampine JP. Naloxone augments muscle sympathetic nerve activity during isometric exercise in humans. *Am J Physiol Endocrinol Metab* 260: E379–E388, 1991. doi:10.1152/ajpendo.1991.260.3.E379.

Folkow B. Perspectives on the integrative functions of the 'sympatho-adrenomedullary system'. *Auton Neurosci* 83: 101–115, 2000. doi:10.1016/S1566-0702(00)00171-5.

Gregor M, Jänig W, Riedel W. Response pattern of cutaneous postganglionic neurones to the hindlimb on spinal cord heating and cooling in the cat. *Pflugers Arch* 363: 135–140, 1976. doi:10.1007/BF01062281.

Hainsworth R. Cardiovascular control from cardiac and pulmonary vascular receptors. *Exp Physiol* 99: 312–319, 2014. doi:10.1113/expphysiol.2013.072637.

Hardy JC, Gray K, Whisler S, Leuenberger U. Sympathetic and blood pressure responses to voluntary apnea are augmented by hypoxemia. *J Appl Physiol (1985)* 77: 2360–2365, 1994. doi:10.1152/jappl.1994.77.5.2360.

Horeyseck G, Jänig W, Kirchner F, Thämer V. Activation and inhibition of muscle and cutaneous postganglionic neurones to hindlimb during hypothalamically induced vasoconstriction and atropine-sensitive vasodilation. *Pflugers Arch* 361: 231–240, 1976. doi:10.1007/BF00587287.

Incognito AV, Doherty CJ, Nardone M, Lee JB, Notay K, Seed JD, Millar PJ. Evidence for differential control of muscle sympathetic single units during mild sympathoexcitation in young, healthy humans. *Am J Physiol Heart Circ Physiol* 316: H13–H23, 2019. doi:10.1152/ajpheart.00675.2018.

Incognito AV, Samora M, Shepherd AD, Cartafina RA, Guimarães GM, Daher M, Millar PJ, Vianna LC. Arterial baroreflex regulation of muscle sympathetic single-unit activity in men: influence of resting blood pressure. *Am J Physiol Heart Circ Physiol* 318: H937–H946, 2020. doi:10.1152/ajpheart.00700.2019.

Inglis EC, Iannetta D, Murias JM. The plateau in the NIRS-derived [HHb] signal near the end of a ramp incremental test does not indicate the upper limit of O_2 extraction in the vastus lateralis. *Am J Physiol Regul Integr Comp Physiol* 313: R723–R729, 2017. doi:10.1152/ajpregu.00261.2017.

Katayama K, Ishida K, Saito M, Koike T, Ogoh S. Hypoxia attenuates cardiopulmonary reflex control of sympathetic nerve activity during mild dynamic leg exercise. *Exp Physiol* 101: 377–386, 2016. doi:10.1113/EP085632.

Katayama K, Kaur J, Young BE, Barbosa TC, Ogoh S, Fadel PJ. High-intensity muscle metaboreflex activation attenuates cardiopulmonary baroreflex-mediated inhibition of muscle sympathetic nerve activity. *J Appl Physiol (1985)* 125: 812–819, 2018. doi:10.1152/japplphysiol.00161.2018.

Klassen SA, Limberg JK, Baker SE, Nicholson WT, Curry TB, Joyner MJ, Shoemaker JK. The role of the paravertebral ganglia in human sympathetic neural discharge patterns. *J Physiol* 596: 4497–4510, 2018. doi:10.1113/JP276440.

Klassen SA, Moir ME, Usselman CW, Shoemaker JK. Heterogeneous baroreflex control of sympathetic action potential subpopulations in humans. *J Physiol* 598: 1881–1895, 2020. doi:10.1113/JP279326.

Limberg JK, Ott EP, Holbein WW, Baker SE, Curry TB, Nicholson WT, Joyner MJ, Shoemaker JK. Pharmacological assessment of the contribution of the arterial baroreflex to sympathetic discharge patterns in healthy humans. *J Neurophysiol* 119: 2166–2175, 2018. doi:10.1152/jn.00935.2017.

Lovick TA. Differential control of cardiac and vasomotor activity by neurones in nucleus paragigantocellularis lateralis in the cat. *J Physiol* 389: 23–35, 1987. doi:10.1113/jphysiol.1987.sp016644.

Macefield VG, Elam M, Wallin BG. Firing properties of single postganglionic sympathetic neurones recorded in awake human subjects. *Auton Neurosci* 95: 146–159, 2002. doi:10.1016/S1566-0702(01)00389-7.

Macefield VG, Wallin BG. Physiological and pathophysiological firing properties of single postganglionic sympathetic neurons in humans. *J Neurophysiol* 119: 944–956, 2018. doi:10.1152/jn.00004.2017.

Mark AL, Victor RG, Nerhed C, Wallin BG. Microneurographic studies of the mechanisms of sympathetic nerve responses to static exercise in humans. *Circ Res* 57: 461–469, 1985. doi:10.1161/01.RES.57.3.461.

McAllen RM, Dampney RA. Vasomotor neurons in the rostral ventrolateral medulla are organized topographically with respect to type of vascular bed but not body region. *Neurosci Lett* 110: 91–96, 1990. doi:10.1016/0304-3940(90)90793-9.

McAllen RM, May CN, Shafton AD. Functional anatomy of sympathetic premotor cell groups in the medulla. *Clin Exp Hypertens* 17: 209–221, 1995. doi:10.3109/10641969509087066.

McDougall SJ, Andresen MC. Independent transmission of convergent visceral primary afferents in the solitary tract nucleus. *J Neurophysiol* 109: 507–517, 2013. doi:10.1152/jn.00726.2012.

McDougall SJ, Peters JH, Andresen MC. Convergence of cranial visceral afferents within the solitary tract nucleus. *J Neurosci* 29: 12886–12895, 2009. doi:10.1523/JNEUROSCI.3491-09.2009.

Meckler RL, Weaver LC. Characteristics of ongoing and reflex discharge of single splenic and renal sympathetic postganglionic fibres in cats. *J Physiol* 396: 139–153, 1988. doi:10.1113/jphysiol.1988.sp016955.

Millar PJ, Murai H, Floras JS. Paradoxical muscle sympathetic reflex activation in human heart failure. *Circulation* 131: 459–468, 2015. doi:10.1161/CIRCULATIONAHA.114.010765.

Millar PJ, Murai H, Morris BL, Floras JS. Microneurographic evidence in healthy middle-aged humans for a sympathoexcitatory reflex activated by atrial pressure. *Am J Physiol Heart Circ Physiol* 305: H931–H938, 2013. doi:10.1152/ajpheart.00375.2013.

Morrison SF. Differential control of sympathetic outflow. *Am J Physiol Regul Integr Comp Physiol* 281: R683–R698, 2001. doi:10.1152/ajpregu.2001.281.3.R683.

Mueller PJ, Mischel NA, Scislo TJ. Differential activation of adrenal, renal, and lumbar sympathetic nerves following stimulation of the rostral ventrolateral medulla of the rat. *Am J Physiol Regul Integr Comp Physiol* 300: R1230–R1240, 2011. doi:10.1152/ajpregu.00713.2010.

Murai H, Takamura M, Maruyama M, Nakano M, Ikeda T, Kobayashi D, Otowa K, Ootsuji H, Okajima M, Furusho H, Takata S, Kaneko S. Altered firing pattern of single-unit muscle sympathetic nerve activity during handgrip exercise in chronic heart failure. *J Physiol* 587: 2613–2622, 2009. doi:10.1113/jphysiol.2009.172627.

Murai H, Takata S, Maruyama M, Nakano M, Kobayashi D, Otowa K, Takamura M, Yuasa T, Sakagami S, Kaneko S. The activity of a single muscle sympathetic vasoconstrictor nerve unit is affected by physiological stress in humans. *Am J Physiol Heart Circ Physiol* 290: H853–H860, 2006. doi:10.1152/ajpheart.00184.2005.

Notay K, Seed JD, Incognito AV, Doherty CJ, Nardone M, Burns MJ, Millar PJ. Validity and reliability of measuring resting muscle sympathetic nerve activity using short sampling durations in healthy humans. *J Appl Physiol (1985)* 121: 1065–1073, 2016. doi:10.1152/japplphysiol.00736.2016.

Oberg B, Thorén P. Increased activity in left ventricular receptors during hemorrhage or occlusion of caval veins in the cat. A possible cause of the vaso-vagal reaction. *Acta Physiol Scand* 85: 164–173, 1972. doi:10.1111/j.1748-1716.1972.tb05247.x.

Oberg B, Thorén P. Circulatory responses to stimulation of medullated and non-medullated afferents in the cardiac nerve in the cat. *Acta Physiol Scand* 87: 121–132, 1973. doi:10.1111/j.1748-1716.1973.tb05373.x.

Paton JF. The Sharpey-Schafer prize lecture: nucleus tractus solitarii: integrating structures. *Exp Physiol* 84: 815–833, 1999. doi:10.1111/j.1469-445X.1999.01912.x.

Riedel W, Peter W. Non-uniformity of regional vasomotor activity indicating the existence of 2 different systems in the sympathetic cardiovascular outflow. *Experientia* 33: 337–338, 1977. doi:10.1007/BF02002814.

Ross CA, Ruggiero DA, Reis DJ. Projections from the nucleus tractus solitarii to the rostral ventrolateral medulla. *J Comp Neurol* 242: 511–534, 1985. doi:10.1002/cne.902420405.

Salmanpour A, Brown LJ, Steinback CD, Usselman CW, Goswami R, Shoemaker JK. Relationship between size and latency of action potentials in human muscle sympathetic nerve activity. *J Neurophysiol* 105: 2830–2842, 2011. doi:10.1152/jn.00814.2010.

Salmanpour A, Shoemaker JK. Baroreflex mechanisms regulating the occurrence of neural spikes in human muscle sympathetic nerve activity. *J Neurophysiol* 107: 3409–3416, 2012. doi:10.1152/jn.00925.2011.

Scherrer U, Vissing S, Morgan BJ, Hanson P, Victor RG. Vasovagal syncope after infusion of a vasodilator in a heart-transplant recipient. *N Engl J Med* 322: 602–604, 1990. doi:10.1056/NEJM199003013220906.

Seagard JL, Hopp FA, Drummond HA, Van Wynsberghe DM. Selective contribution of two types of carotid sinus baroreceptors to the control of blood pressure. *Circ Res* 72: 1011–1022, 1993. doi:10.1161/01.RES.72.5.1011.

Seals DR, Johnson DG, Fregosi RF. Hypoxia potentiates exercise-induced sympathetic neural activation in humans. *J Appl Physiol (1985)* 71: 1032–1040, 1991. doi:10.1152/jappl.1991.71.3.1032.

Shoemaker JK. Recruitment strategies in efferent sympathetic nerve activity. *Clin Auton Res* 27: 369–378, 2017. doi:10.1007/s10286-017-0459-x.

Simon E, Riedel W. Diversity of regional sympathetic outflow in integrative cardiovascular control: patterns and mechanisms. *Brain Res* 87: 323–333, 1975. doi:10.1016/0006-8993(75)90429-1.

Simpson LL, Meah VL, Steele A, Thapamagar S, Gasho C, Anholm JD, Drane AL, Dawkins TG, Busch SA, Oliver SJ, Lawley JS, Tymko MM, Ainslie PN, Steinback CD, Stembridge M, Moore JP. Evidence for a physiological role of pulmonary arterial baroreceptors in sympathetic neural activation in healthy humans. *J Physiol* 598: 955–965, 2020. doi:10.1113/JP278731.

Somers VK, Mark AL, Abboud FM. Interaction of baroreceptor and chemoreceptor reflex control of sympathetic nerve activity in normal humans. *J Clin Invest* 87: 1953–1957, 1991. doi:10.1172/JCI115221.

Steinback CD, Salmanpour A, Breskovic T, Dujic Z, Shoemaker JK. Sympathetic neural activation: an ordered affair. *J Physiol* 588: 4825–4836, 2010. doi:10.1113/jphysiol.2010.195941.

Sundlöf G, Wallin BG. Effect of lower body negative pressure on human muscle nerve sympathetic activity. *J Physiol* 278: 525–532, 1978. doi:10.1113/jphysiol.1978.sp012322.

Teixeira AL, Fernandes IA, Vianna LC. Cardiovascular control during exercise: the connectivity of skeletal muscle afferents to the brain. *Exerc Sport Sci Rev* 48: 83–91, 2020. doi:10.1249/JES.0000000000000218.

Wallin BG, Eckberg DL. Sympathetic transients caused by abrupt alterations of carotid baroreceptor activity in humans. *Am J Physiol* 242: H185–H190, 1982. doi:10.1152/ajpheart.1982.242.2.H185.

Zera T, Moraes DJ, da Silva MP, Fisher JP, Paton JF. The logic of carotid body connectivity to the brain. *Physiology (Bethesda)* 34: 264–282, 2019. doi:10.1152/physiol.00057.2018.